Analytical equivalent models of artificial dielectric layers with arbitrary inter-layer shifts

Cavallo, Daniele

Publication date
2018

Document Version
Accepted author manuscript

Published in
12th European Conference on Antennas and Propagation, EuCAP 2018

Analytical Equivalent Models of Artificial Dielectric Layers with Arbitrary Inter-Layer Shifts

Daniele Cavallo[1],
[1] Microelectronics Department, Delft University of Technology, Delft, The Netherlands, d.cavallo@tudelft.nl

***Abstract*—Closed-form expressions to describe artificial dielectric layers (ADLs) are presented. The propagation of a generic plane wave within the artificial material is described by means of transmission line models, where each layer is represented as an equivalent shunt impedance. The given analytical formulas for the shunt impedance account for the reactive coupling between the layers due to higher order Floquet modes, thus remain valid even for extremely small electrical distance between layers. The expressions are derived assuming finite conductivity of the metal, thus also an accurate estimation of the losses within the artificial dielectric is obtained from the equivalent circuit.**

***Index Terms*—Artificial dielectric layers, closed-form solutions, equivalent circuit.**

I. Introduction

Several of today's radar and wireless communication applications are shifting their operation to higher frequency to fulfill more demanding requirements on resolution, compactness and data rates. When the operating frequency of these systems increases, reaching the millimeter and sub-millimeter waves, the separation of antenna and electronic circuits is no longer possible. Thus, the recent trend is to place the antennas as close as possible to the the electronic components, to facilitate the interconnection and to realize highly integrated front-ends. Despite this need, integrated antennas have never showed good performance because of their intrinsic low efficiency. These antennas are limited by problems such as high surface-wave loss, narrow bandwidth, low front-to-back radiation ratio [1].

Recently, an approach to greatly improve the efficiency of integrated antennas was proposed in [2], [3]. It consists of adding an artificial dielectric slab above the antenna in order to increase the front-to-back ratio. Because of the anisotropy of the artificial dielectric, surface waves are not excited, thus resulting in very high radiation efficiency.

A closed-form analysis of artificial dielectric layers (ADLs) was presented in [4], [5], valid for aligned layers (Fig. 1(a)), and subsequently generalized in [6] to include the shift between even and odd layers (Fig. 1(b)). Although Fig. 1(b) depicts the case of maximum shift (layers are shifted by half of the period), the shift can be an arbitrary percentage of the unit cell size, realizing an example of glide symmetric structure. It was shown in [6] that the shift greatly increases the effective relative permittivity of the artificial dielectric with respect to the aligned case, thus it constitutes a key parameter for more flexible ADL designs.

All previous works consider lossless patches, made of perfect electric conductor. The assessment of the losses in ADL was never included before in the analysis. Losses in ADLs are typically very small because of the sub-wavelength dimensions of the patches, that yield very low current intensity on each patch. However, these losses can vary depending on how the ADL slab is illuminated, e.g. by a near source or under plane-wave incidence, and they also depend on the polarization and direction of the incident field. For these reasons, it is useful to include the finite conductivity of the metal already in the analytical formulas, to accurately quantify the losses and give more physical insight on the nature of Ohmic dissipation in ADLs. In this work the losses introduced by the finite conductivity of the metal patches in ADLs are analytically characterized, to derive an effective dissipation factor ($\tan\delta$) for these structure.

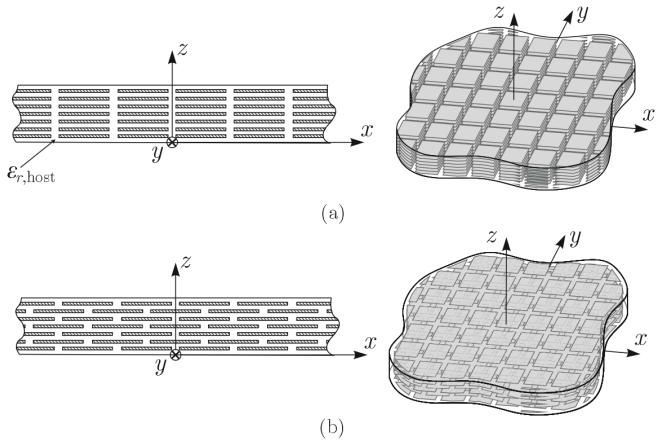

Fig. 1. Two-dimensional side view and three-dimensional prospective view for artificial dielectric slabs with (a) aligned and (b) shifted layers.

II. Single Layer with Finite Conductivity

A. Equivalence Theorem and Integral Equation

The initial problem under consideration is a layer of periodic square patches in the x-y plane, infinitely thin in z and illuminated by a generic plane wave with electric and magnetic fields $\mathbf{e}_i$ and $\mathbf{h}_i$. The unit cell of the patch array is shown in Fig. 2(a) and it is characterized by period d and width of the slots w. Due to finite conductivity σ, the metal can be described by a surface impedance Z_s, which is given by

$$Z_s = (1+j)\sqrt{\frac{k_0\zeta_0}{2\sigma}} \tag{1}$$

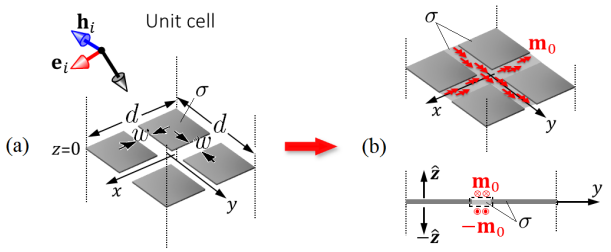

Fig. 2. (a) Unit cell of a single layer of periodic square patches illuminated by a plane wave. (b) Equivalent problem with magnetic surface current on the gaps.

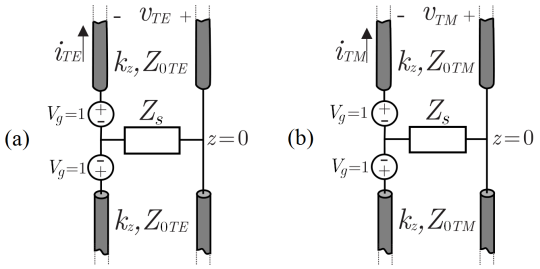

Fig. 3. Equivalent z-transmission lines for the spectral Green's function of the problem: (a) TE and (b) TM modes.

where k_0 and ζ_0 are the free-space wavenumber and impedance, respectively.

The metal surface is modeled using the Leontovich boundary conditions: $\mathbf{e}\times\hat{\mathbf{n}} = Z_s\hat{\mathbf{n}}\times[\mathbf{h}\times\hat{\mathbf{n}}]$, where $\hat{\mathbf{n}}$ is the outward normal unit vector of the surface, and the fields $\mathbf{e}$ and $\mathbf{h}$ denote the total fields, equal to the sum of incident and scattered. By applying the equivalence theorem, the gaps between patches are enclosed with infinitely thin closed surfaces, with equivalent electric and magnetic surface current densities $\mathbf{j}_0$ and $\mathbf{m}_0$ above and below. The equivalent currents are related to the fields by $\mathbf{j}_0 = \hat{\mathbf{n}}\times\mathbf{h}$ and $\mathbf{m}_0 = \mathbf{e}\times\hat{\mathbf{n}}$.

Following a procedure similar to [7], the volume enclosed by the surface can be filled with a material which has the same finite conductivity as the metal patches, to obtain an homogeneous layer that is convenient to represent with spectral Green's function of stratified media. An effective magnetic current density $\mathbf{m}_e$, that account for both $\mathbf{j}_0$ and $\mathbf{m}_0$, can be defined as

$$\mathbf{m}_e = \mathbf{m}_0 + \mathbf{m}_\mathbf{j} = \mathbf{m}_0 + Z_s\hat{\mathbf{n}}\times\mathbf{j}_0\,. \tag{2}$$

The continuity of both electric and magnetic fields in the gap implies that the currents above and below the layer are equal and with opposite signs for $\mathbf{m}_0$, but with same sign for $\mathbf{m}_\mathbf{j}$:

$$\mathbf{m}_0^+ = \mathbf{e}^+\times\hat{\mathbf{z}} = \mathbf{e}^-\times(-\hat{\mathbf{z}}) = -\mathbf{m}_0^+ \tag{3}$$

$$\mathbf{m}_\mathbf{j}^+ = Z_s\,\hat{\mathbf{z}}\times(\hat{\mathbf{z}}\times\mathbf{h}^+) = Z_s(-\hat{\mathbf{z}})\times(-\hat{\mathbf{z}}\times\mathbf{h}^-) = \mathbf{m}_\mathbf{j}^- \tag{4}$$

where the superscripts '+' and '−' are used to indicate the current or the field above and below the layer plane. Thus, by imposing the continuity of the tangential magnetic field in the gaps, the following integral equation can be defined:

$$\int_{-\infty}^{\infty}\int_{-\infty}^{\infty} 2\mathbf{m}_0(\boldsymbol{\rho}')\mathbf{g}_{Z_s}(\boldsymbol{\rho}-\boldsymbol{\rho}')d\boldsymbol{\rho}' = -(1+\Gamma)\mathbf{h}_\mathrm{i} \tag{5}$$

where Γ is the reflection coefficient of the magnetic field at the metal, $\boldsymbol{\rho} = x\hat{\mathbf{x}}+y\hat{\mathbf{y}}$ and $\boldsymbol{\rho}' = x'\hat{\mathbf{x}}+y'\hat{\mathbf{y}}$ are the observation and source points respectively, and $\mathbf{g}_{Z_s}$ is the Green's function that relates the elementary magnetic source located on the infinite lossy plane to the magnetic field. One can note that the magnetic current $\mathbf{m}_\mathbf{j}$ does not contribute to the magnetic field integral equation, since the difference between the field scattered above and below by $\mathbf{m}_\mathbf{j}$ vanishes. Therefore, the integral equation can be written only in terms of magnetic current density $\mathbf{m}_0$. This is because, unlike [7], the Green's functions for the currents above and below the layer are the same in the problem under analysis.

Equation (5) can be solved by an appropriate expansion of the magnetic current in four entire domain basis functions, defined on the entire unit cell, and by Galerkin projection, as described in [4]. The terms of the admittance matrix are conveniently calculated in the spectral domain. For this reason, the spectral Green's function is derived in terms of the current i on transmission lines shown in Fig. 3, for transverse electric (TE) and transverse magnetic (TM) modes. The magnetic current sources are represented by unit voltage generators. The characteristic impedance of the transmission lines are $Z_{0TE} = \zeta_0 k_0/k_z$ and $Z_{0TM} = \zeta_0 k_z/k_0$ where k_z is $(k_0^2 - k_x^2 - k_y^2)^{1/2}$. The variables k_x and k_y indicate the spectral counterparts of the spatial variables x and y.

B. Equivalent Layer Impedance

After the Green's function is obtained, the rest of the steps are very similar to the lossless case [4], thus omitted here. The procedure leads to the following expression for the equivalent layer impedance:

$$Z_{\text{layer,TE}} = \frac{1}{Y_{TE}} + Z_s, \qquad Z_{\text{layer,TM}} = \frac{1}{Y_{TM}} + Z_s \tag{6}$$

where Y_{TE} and Y_{TM} are no longer pure susceptances as in the lossless case, but they are given by

$$Y_{TE} \approx 2\sum_{m_y\neq 0}|\mathrm{sinc}(k_{ym}w/2)|^2 \left(\frac{k_{x0}^2}{2k_{ym}^2}\left(\frac{\zeta_0 k_0}{k_{zm}}+2Z_s\right)^{-1}+\left(\frac{\zeta_0 k_{zm}}{k_0}+2Z_s\right)^{-1}\right) \tag{7}$$

$$Y_{TM} \approx 2\sum_{m_x\neq 0}|\mathrm{sinc}(k_{xm}w/2)|^2 \left(\frac{k_{y0}^2}{k_{xm}^2}\left(\frac{\zeta_0 k_0}{k_{zm}}+2Z_s\right)^{-1}+\left(\frac{\zeta_0 k_{zm}}{k_0}+2Z_s\right)^{-1}\right) \tag{8}$$

where m_x and m_y are the indexes of the Floquet modes, $k_{xm} = k_{x0} - 2\pi m_x/d$ and $k_{ym} = k_{y0} - 2\pi m_y/d$ are the

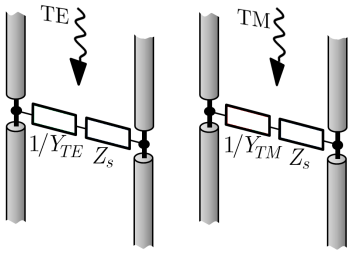

Fig. 4. Equivalent circuit representation of the single layer of patches with finite conductivity.

Floquet wavenumbers, which determine $k_{zm} = (k_0^2 - k_{xm}^2 - k_{ym}^2)^{1/2}$; $k_{x0} = k_0 \sin\theta\cos\phi$ and $k_{y0} = k_0 \sin\theta\sin\phi$ are the propagation constant of the incident plane wave along x and y, respectively. Equations (6), (7) and (8) are valid for the lossless case, by imposing $Z_s = 0$.

Figure 4 shows the equivalent circuit representation of the impedance, including the Z_s contribution. The finite conductivity introduces an impedance term (Z_s) that is in series with the layer impedance. However, the term Z_s is not the only contribution to the resistance, as also the impedances $1/Y_{TE}$ $1/Y_{TM}$ have a comparable resistive component.

To quantify the effect of the finite conductivity, the losses are defined as

$$\text{Loss}(dB) = 10\log_{10}\frac{1}{|S_{11}|^2 + |S_{12}|^2} \tag{9}$$

where S_{11} and S_{12} are reflection and transmission coefficient of the incident plane wave, respectively. To validate the analytical solutions, Fig. 5 compares the losses obtained with the analytical solution and HFSS simulations, showing good agreement. Since the losses of the structure with realistic conductivity values are negligible, an unrealistically low conductivity of $\sigma = 1000$ S/m is taken for the validation. The geometrical parameters are $d = 0.095\lambda_0$ and $w = 0.01\lambda_0$, with λ_0 being the wavelength at 300 GHz. The incident plane wave is impinging at oblique angles ($\theta = 40°, \phi = 0°$ and $\theta = 60°, \phi = 0°$).

It is evident that the loss calculated for TE incidence is generally larger than the value observed for TM incidence. This phenomenon likely happens due to the occurrence of electric current loops that are supported by the patches when the structure is illuminated by TE incidence. Figure 6(a) shows the electric field distribution on the single layer for TE incidence, and the correspondent electric current on the patches forming a loop. A TM incidence is instead not supporting such current loops, but only excites uniform and singly polarized currents on the patches, as shown in Fig. 6(b). The current loops are associated with a longer electrical length, and therefore with higher current intensity (closer to the resonance), which can explain the increased Ohmic losses.

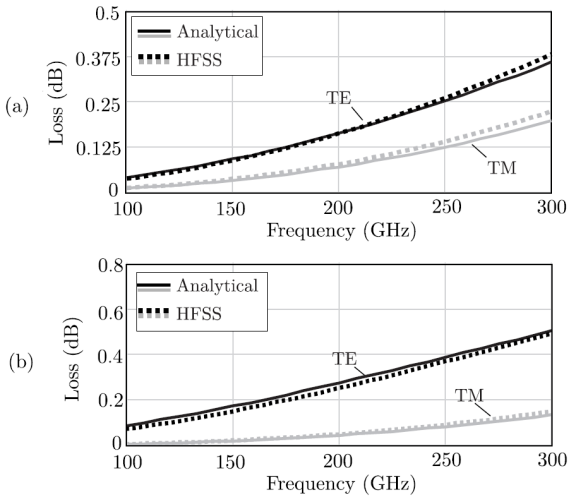

Fig. 5. Comparing loss (in dB) calculated based on analytical solution and HFSS simulation. The plane wave incident on a single layer of patches with finite conductivity ($\sigma = 1000$ S/m) with angle of incidence: (a) $\theta = 40°$, $\phi = 0°$; (b) $\theta = 60°$, $\phi = 0°$. The geometrical parameters are $d = 0.095\lambda_0$ and $w = 0.01\lambda_0$, with λ_0 being the wavelength at 300 GHz.

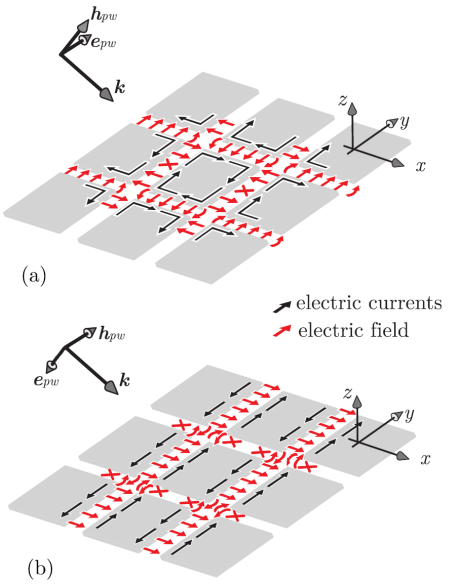

Fig. 6. Illustration on single layer of periodic patches illuminated by TE incidence. The electric fields that are propagating in the slot generate electric current loops in the patches.

III. Multiple Layer with Finite Conductivity

Following the same generalization procedure used in [5], [6], the analysis can be expanded to account for a finite cascade of layers. This allows to quantify analytically the losses in ADLs already in the early phase of the design process. The steps are omitted, as they are similar to the ones described in the previous publications. We consider a plane wave incident on a finite cascade of layers with arbitrary shift between even and odd layers (indicated by s, equal along x and

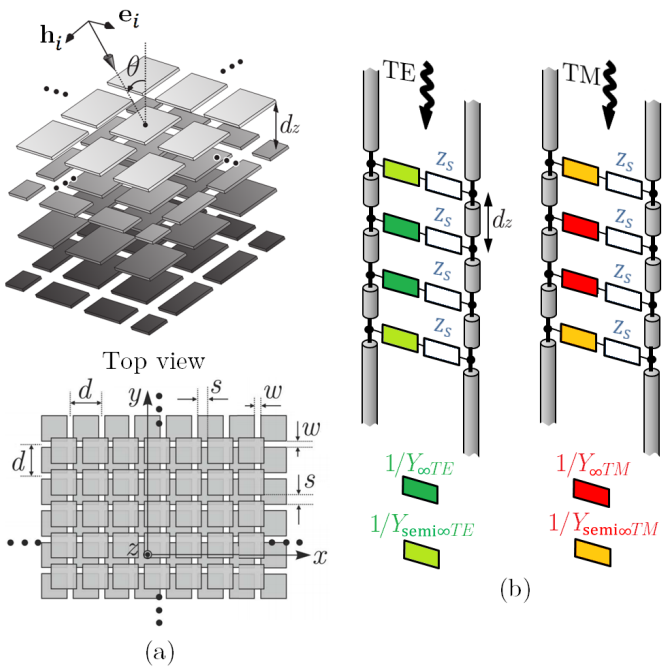

Fig. 7. Equivalent circuit representation of the ADL composed of 5 layers with finite conductivity for TE and TM component.

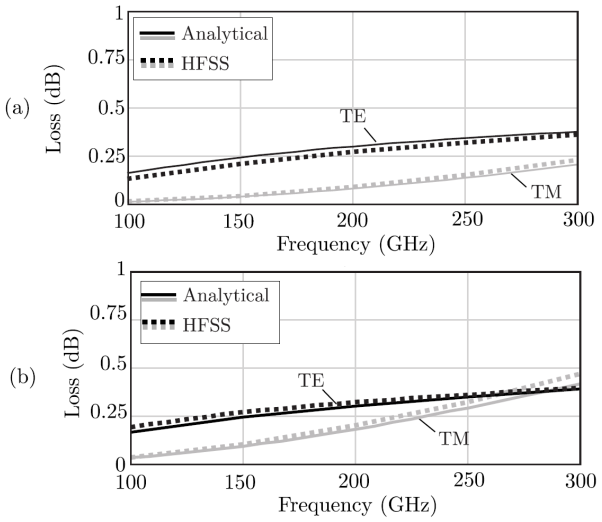

Fig. 8. Comparing losses calculated based on analytical solution and HFSS simulation. The plane wave is incident on a three-layer ADL with finite conductivity ($\sigma = 1000$ S/m) with angle of incidence $\theta = 60°$, $\phi = 0°$. The geometrical parameters are $d = 0.095\lambda_0$, $w = 0.01\lambda_0$, $d_z = 0.02\lambda_0$, with λ_0 being the wavelength at 300 GHz, and shift (a) $s = 0$ (aligned) and (b) $s = d/2$.

y), as shown in Fig. 7(a). The equivalent circuit representation in Fig. 7(b) can be used, where the admittances of the layers are separated into infinite-cascade and semi-infinite-cascade solutions, to describe the middle layers and the layers at the edges, respectively. To account for the reactive coupling between layers, the admittances terms in (7) and (8) are now generalized as follows:

$$Y_{\infty TE} \approx 2 \sum_{m_y \neq 0} |\text{sinc}(k_{ym} w/2)|^2 S_\infty \left(\frac{k_{x0}^2}{2k_{ym}^2} \left(\frac{\zeta_0 k_0}{k_{zm}} + 2Z_s S_\infty \right)^{-1} + \left(\frac{\zeta_0 k_{zm}}{k_0} + 2Z_s S_\infty \right)^{-1} \right) \quad (10)$$

$$Y_{\infty TM} \approx 2 \sum_{m_x \neq 0} |\text{sinc}(k_{xm} w/2)|^2 S_\infty \left(\frac{k_{y0}^2}{k_{xm}^2} \left(\frac{\zeta_0 k_0}{k_{zm}} + 2Z_s S_\infty \right)^{-1} + \left(\frac{\zeta_0 k_{zm}}{k_0} + 2Z_s S_\infty \right)^{-1} \right) \quad (11)$$

where we introduced the term S_∞ given by

$$S_\infty = -j \cot\left(\frac{-j2\pi|m|d_z}{d}\right) + j e^{j2\pi m \frac{s}{d}} \csc\left(\frac{-j2\pi|m|d_z}{d}\right). \quad (12)$$

The admittances for the edge layers (first and last layer) have the same expressions, but replacing S_∞ with $S_{\text{semi}\infty}$:

$$S_{\text{semi}\infty} = \frac{1}{2} - \frac{j}{2} \cot\left(\frac{-j2\pi|m|d_z}{d}\right) + \frac{j}{2} e^{j2\pi m \frac{s}{d}} \csc\left(\frac{-j2\pi|m|d_z}{d}\right). \quad (13)$$

Full-wave HFSS simulations are made to validate the analytical solution, and the comparison is shown in Fig. 8. A good agreement can be seen for the cases shown. Figures 8(a) and (b) refer to a cascade of three layers with $\sigma = 1000$ S/m, aligned and shifted respectively. The geometrical parameters are $d = 0.095\lambda_0$, $w = 0.01\lambda_0$ and $d_z = 0.02\lambda_0$, with λ_0 being the wavelength at 300 GHz. The incident plane wave is incoming at oblique angle ($\theta = 60°, \phi = 0°$). It can be observed that the shift does not introduce a significant increase of losses, despite providing much higher equivalent permittivity compared to the aligned case. The loss for TE incidence shown in Figs. 8(a) and (b) appear not to increase with the frequency as the TM case. This observation can be explained with the fact that the transmission coefficient for the TE case decreases significantly as the frequency grows. The low transmission signifies that most of the incident wave is reflected at the interface between the air and the ADL, thus interacts less with the lossy metal patches.

Figure 9 shows a case where the ADL is designed so the total height of the slab becomes resonant (half of the effective wavelength) within the frequency of investigation. The ADL comprises 5 layers with conductivity $\sigma = 10^6$S/m with the same geometrical parameters as in Fig. 8, except for the interelement spacing $d_z = 0.15\lambda_0$. It can be observed that the losses are maximum around 250 GHz, which also corresponds to the maximum transmission of the slabs. This effect can be interpreted by imagining that, at the resonance, the wave undergoes multiple bounces within the material which add up in phase in the transmitted wave, resulting in higher losses.

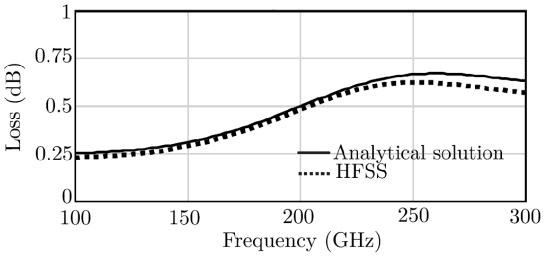

Fig. 9. Losses for TE incidence from the direction $\theta = 60°$, $\phi = 0°$ on a 5-layer aligned ADL with conductivity $\sigma = 10^6$ S/m. The geometrical parameters are $d = 0.095\lambda_0$, $w = 0.01\lambda_0$, $d_z = 0.15\lambda_0$, with λ_0 being the wavelength at 300 GHz.

IV. Conclusion

We presented analytical formulas to describe artificial dielectric layers where the metal patches are characterized by finite conductivity. In this way, the losses are taken into account rigorously in the closed form expressions of the equivalent layer impedance. The geometry investigated is an example of glide symmetric structure, since the even layers of the artificial dielectric can be arbitrarily shifted with respect to the odd ones. The analytical spectral Green's function provided here is useful to design artificial dielectric layers as standalone material or in combination with antennas located in the near field.

References

[1] D. Cavallo, W. H. Syed and A. Neto, "Artificial dielectric enabled antennas for high frequency radiation from integrated circuits," *11th Eur. Conf. Antennas Propagation*, Paris, 2017, pp. 1626-1628.

[2] W. H. Syed and A. Neto, "Front-to-back ratio enhancement of planar printed antennas by means of artificial dielectric layers," *IEEE Trans. Antennas Propag.*, vol. 61, no. 11, pp. 5408-5416, Nov. 2013.

[3] W. H. Syed, G. Fiorentino, D. Cavallo, M. Spirito, P. M. Sarro, and A. Neto, "Design, fabrication and measurement of 0.3 THz on-chip double-slot antenna enhanced by artificial dielectrics," *IEEE Trans. THz Sci. Tech.*, vol. 5, no. 2, pp. 288-298, Mar. 2015.

[4] D. Cavallo, W. H. Syed, and A. Neto, "Closed-form analysis of artificial dielectric layers−Part I: Properties of a single layer under plane-wave incidence," *IEEE Trans. Antennas Propag.*, vol. 62, no. 12, pp. 6256-6264, Dec. 2014.

[5] D. Cavallo, W. H. Syed, and A. Neto, "Closed-form analysis of artificial dielectric layers−Part II: Extension to multiple layers and arbitrary illumination," *IEEE Trans. Antennas Propag.*, vol. 62, no. 12, pp. 6265-6273, Dec. 2014.

[6] D. Cavallo and C. Felita, "Analytical formulas for artificial dielectrics with nonaligned layers," *IEEE Transactions on Antennas and Propagation*, vol. 65, no. 10, pp. 5303-5311, Oct. 2017.

[7] M. Albani, A. Mazzinghi and A. Freni, "Rigorous MoM analysis of finite conductivity effects in RLSA antennas," *IEEE Transactions on Antennas and Propagation*, vol. 59, no. 11, pp. 4023-4032, Nov. 2011.